

Quenching studies in the high-pressure CTAC phase reveal a significant difference in the pressure effect. The plot in Figure 4 gives $\Delta V_q^* = 7.9 \text{ cm}^3 \text{ mol}^{-1}$ in the micellar phase, as already found at 23 °C, and a pressure-independent k_q above the phase transition. Table II summarizes the lifetime and quenching data for the two CTAC phases. The slight decrease in k_q and the large decrease in τ_0 above the phase transition are evident from Figures 4 and 1, respectively. Also given in Table II are the pyrene fluorescence peak ratios I_1/I_3 which are related to the polarity of the microenvironment. A low I_1/I_3 ratio implies a nonpolar environment. As previously observed¹⁴ the I_1/I_3 intensity ratio in CTAC micellar solutions is unaltered by pressure but decreases 20% at the phase transition. Further compression of the ordered phase increases I_1/I_3 , as observed for τ_0 .

Discussion

This study of pyrene quenching supports the view that the probe remains in partial contact with water at all pressures. The ΔV_q^* 's are intermediate between those expected for encounter-controlled reactions in aqueous and hydrocarbon environments, as predicted by eq 2. The values of 7-8 $\text{cm}^3 \text{ mol}^{-1}$ in CTAC micellar solutions (Table I) are comparable in magnitude to $\Delta V_q^* = 7.7 \text{ cm}^3 \text{ mol}^{-1}$ reported for the pyrene/*m*-DCNB/ CH_3CN system.⁹ Use of eq 3 gives $\Delta V_q^* \approx \text{cm}^3 \text{ mol}^{-1}$ for the CTAC data obtained by Turro and Okubo,¹⁰ using the intramolecular excimer technique. Dodecane viscosity data¹⁹ give $\Delta V_q^* \approx 22 \text{ cm}^3 \text{ mol}^{-1}$. These results are persuasive, indicating that the micellar microenvironment of pyrene is characterized by a balance between hydrocarbon and water contacts.

The transition from micelle to ordered phase at the solubility limit is expected to increase hydrocarbon order and to expel water and pyrene from the interior toward the bilayer surface. The large contrast in ΔV_q^* for the two phases (Table II) suggests that pyrene is buried deep and accessible to water in the micellar phase, as envisioned for the Menger micelle.²⁰ The k_q values remain low upon precipitation, as well as electrolyte addition, because increased order of the water structure near the vicinity of the probe site increases the local viscosity.

The lifetime and intensity (I_1/I_3) data across the surfactant and dodecane phase transitions cannot be related to solvent polarity effects but must be attributed to packing strain identified with the pressure parameter. Thus the large decrease of 40% and 30% measured across the dodecane freezing curve can only represent a response to the pressure-induced distortion of the probe site. Similarly, the large discontinuity in τ_0 and I_1/I_3 across the CTAC phase transition can be assigned the same origin. These results suggest that lattice ordering effects are strongly mirrored in the photophysical properties of the pyrene probe molecule.

Since large changes in τ_0 and I_1/I_3 accompany phase discontinuities but not micellar compression, continued disorder and a large wet region in the Menger micelle are indicated.

Acknowledgment. This work is made possible by the financial support of the Department of Chemistry and The Marine Science Institute, by the gift of CTAC from Professor Bunton, and by access to the lifetime instrumentation of Professor Watts.

Registry No. CTAC, 112-02-7; CNP, 100-48-1; *m*-DCNB, 626-17-5; pyrene, 129-00-0; dodecane, 112-40-3.

(19) Hogenboom, D., Webb, W.; Dixon, J. J. *Chem. Phys.* 1967, 46, 2586.

(20) Menger, F. M.; Doll, D. W. *J. Am. Chem. Soc.* 1984, 106, 1109.

Photophysical and Photochemical Deactivation Processes of Ultraviolet Stabilizers of the (2-Hydroxyphenyl)benzotriazole Class

Gottfried Woessner,[†] Gernot Goeller,[†] Petra Kollat,[‡] John J. Stezowski,[‡] Manfred Hauser,[†] Uwe K. A. Klein,[‡] and Horst E. A. Kramer^{*†}

Institut fuer Physikalische Chemie, and Institut fuer Organische Chemie, Biochemie and Isotopenforschung, Universitaet Stuttgart, D-7000 Stuttgart 80, Federal Republic of Germany; and University of Petroleum & Minerals, Dhahran, Saudi Arabia (Received: May 16, 1984)

The X-ray crystal structure determination reveals that TIN (2-(2'-hydroxy-5'-methylphenyl)benzotriazole) is planar with a relatively strong intramolecular hydrogen bond, in which the phenol serves as the donor to a benzotriazole nitrogen. The fluorescence emission of crystalline TIN ($\lambda_{\text{max}} = 638 \text{ nm}$, Stokes shift $\sim 10000 \text{ cm}^{-1}$) is attributed to the S_1' state of the proton transferred species (Figure 4) of TIN with an intramolecular hydrogen bond, in which the benzotriazolium moiety is the donor. The proton transfer yield of deuterated and nondeuterated TIN increases by a factor of two in the range from 296 to 90 K ($\Phi_T \leq 0.5$). The competing process k_d is temperature dependent. No emission from the S_1 state (not proton transferred) was found for crystalline TIN. While the fluorescence lifetime shows the usual isotope effect ($\tau'(D) > \tau'(H)$) no isotope effect on the proton transfer yield was detected (90-350 K).

Introduction

Since the pioneering work of Heller¹ and Heller and Blattmann^{2,3} concerning the photostability of organic compounds the intramolecular hydrogen bond (e.g., *o*-hydroxyphenyl group + hydrogen bond acceptor in the same molecule) has been found to be the most important structural element providing photostability.^{4,5} According to Förster's theory^{6,7} the acidity/basicity of

the intramolecular donor/acceptor group increases upon photoexcitation thus enabling intramolecular proton transfer in the excited state⁸⁻¹² which gives rise to a large Stokes shift in the

(1) Heller, H. J. *Eur. Polym. J.* 1969, 105-132.

(2) Heller, H. J.; Blattmann, H. R. *Pure Appl. Chem.* 1972, 30, 145-165.

(3) Heller, H. J.; Blattmann, H. R. *Pure Appl. Chem.* 1974, 36, 141-161.

(4) Williams, D. L.; Heller, A. J. *Phys. Chem.* 1970, 74, 4473-4480.

(5) Otterstedt, J.-E. A. *J. Chem. Phys.* 1973, 58, 5716-5725.

(6) Förster, Th. Z. *Elektrochem. Angew. Phys. Chem.* 1950, 54, 42-46.

(7) Weller, A. In "Progress of Reaction Kinetics"; Porter, G., Ed.; Pergamon Press: London, 1961; Vol. I, pp 187-214.

[†] Institut fuer Physikalische Chemie.

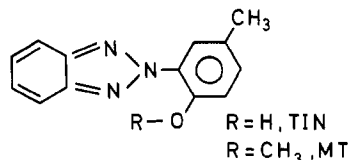
[‡] Institut fuer Organische Chemie.

[‡] University of Petroleum & Minerals.

emission spectrum. In subsequent years the main interest in these substances (widely used as UV stabilizers to diminish photo-degradation of polymers) was focussed on the proton transfer mechanism (thermally activated or tunneling process).^{9,13-19} Shizuka et al. were the first to show by picosecond spectroscopy (stimulated emission and absorption) that intramolecular proton transfer occurs with a rate constant of $1.1 \times 10^{10} \text{ s}^{-1}$ in the S_1 state of 2,4-bis(dimethylamino)-6-(2-hydroxy-5-methylphenyl)-s-triazine;^{14,15} no isotope effect on the proton transfer was found upon deuteration.^{14,15}

Further investigations of intramolecular proton transfer were carried out on *N*-salicylideneanilines,^{17,20,21} on 2-(2'-hydroxyphenyl)benzothiazole,^{18,22,23} on the corresponding benzoxazole,²⁴ on 9-hydroxyphenalenone,²⁵ on methyl salicylate,¹⁹ on *o*-hydroxy-2-naphthoic acids,²⁶ and on various other classes of substances.²⁰ The subsequent transfer of an electron + proton (= hydrogen atom) was observed in an heteroexcimer (pyrene + aromatic amine).²⁷ Gupta et al. and Flom and Barbara studied 2-(2'-hydroxy-5'-methylphenyl)benzotriazole with picosecond spectroscopy in solution^{28,29} and in low-temperature organic glasses.³⁰ In earlier publications we examined the stabilizing effect of 2-(2'-hydroxy-5'-methylphenyl)benzotriazole^{31,32} (trade name Tinuvin P) in poly(*m*-phenyleneisophthalamide), the triplet deactivation and the proton transfer mechanism in the stabilizer molecule (TIN).^{11,12}

In this paper we present measurements of the fluorescence quantum yield and the lifetime of the proton transferred species S_1' at various temperatures for the deuterated and nondeuterated compound with an intramolecular hydrogen bond (TIN(intra)) to gain additional insight into the nature of the proton transfer step; these studies included an X-ray structure analysis.



Experimental Section

Tinuvin P (TIN) was kindly supplied by Dr. Helmut Mueller, CIBA-GEIGY, Basel, Switzerland, and Methyltinuvin (MT) by Prof. Dr. H. Herlinger and Dr. B. Kuester, Institute fuer Textil- und Faserforschung, Wissenschaftliche Institute an der Universitaet Stuttgart, FRG. Both substances were recrystallized three times from *n*-heptane.

Deuteration of the OH Group of TIN. TIN was dissolved in boiling ethanol-*d* together with a catalytic amount of NaOCH_3 and kept at this temperature for 1 h. After cooling the deuterated compound (degree of deuteration >90% as revealed by NMR) precipitated and was recrystallized from *n*-hexane.

Solvents. 2-Methylbutane, *n*-hexane, paraffin oil, ethanol (95%), and dimethyl sulfoxide (Me_2SO) (all from Merck, FRG, spectroscopic grade) were used as supplied. Methylcyclohexane for synthesis (Merck) was purified by an Al_2O_3 column (basic). The hydrocarbon solvents were distilled over P_2O_5 just prior to use. Acetonitrile (analytical grade, Merck) was dried over molecular sieves 3 Å (Merck). Pyridine (analytical grade, Merck) was distilled (no fluorescence). Solvents for low temperature glasses were EEP, ethanol/ether/pyridine 20/20/1 (v); EPA, ether/2-methylbutane/ethanol 5/5/2 (v), and MCH/2-MB, methylcyclohexane/2-methylbutane 1/1 (v).

Crystalline Samples of TIN and MT. Since the relative fluorescence intensities depend on the granulation, the crystalline samples were ground until the highest fluorescence intensity was reached. The crystalline samples were not degassed while those in low-temperature glasses were degassed by the usual freeze-pump-thaw technique.

Samples for Reflection Spectrometry. Solutions of TIN or MT in hydrocarbons were deposited on plates of silica gel (DC, without fluorescence indicator), the mol fraction TIN/SiO_2 being about 10^{-3} mol/kg.

The crystals for the X-ray measurements were obtained by concentrating an *n*-hexane solution. Absorption spectra were registered with a Zeiss DMR absorption spectrometer in the range of 290–350 K; a Cary 14 2/P S/W absorption spectrometer was used for the low-temperature measurements. Cuvettes made of quadratic quartz tube (Heralux Quarzglas) with a pathlength of ca. 10 mm were used.

The relative reflection spectra were measured at the Institute fuer Textil- und Faserforschung, Wissenschaftliche Institute an der Universitaet Stuttgart (Prof. Dr. H. Herlinger and Dr. D. Fiebig) with a Unicam 1800 spectrometer (Philips) equipped for reflection measurements. The calculation of the relative reflection spectra was carried out according to Kortuem et al.³³

Fluorescence and phosphorescence spectra corrected for instrumental sensitivity were measured with a spectrometer described previously (subsequently microcomputerized).^{11,31,34,36} The sensitivity of the instrument was improved. Emissions with a quantum yield of 10^{-6} can be measured while for the recording of an emission excitation spectrum the quantum yield must be $\geq 10^{-4}$. Corrected excitation spectra were obtained with constant excitation intensity controlled by a rhodamine B quantum counter.

- (8) Weller, A. *Z. Elektrochem.* **1956**, *60*, 1144–1147.
 (9) Beens, H.; Grellmann, K. H.; Gurr, M.; Weller, A. *Discuss. Faraday Soc.* **1965**, *39*, 183–193.
 (10) Klöpffer, W. In "Advances in Photochemistry"; Pitts, Jr., J. N., Hammond, G. S., Gollnick, K. Eds.; Wiley: New York, 1977; Vol. 10, pp 311–358.
 (11) Werner, T. *J. Phys. Chem.* **1979**, *83*, pp 320–325.
 (12) Werner, T.; Woessner, G.; Kramer, H. E. A. In "Photodegradation and Photostabilization of Coatings"; Pappas, S. P., Winslow, F. H., Eds.; American Chemical Society: Washington, DC, 1981; ACS Symp. Ser. No. 151, pp 1–18.
 (13) Shizuka, H.; Matsui, K.; Okamura, T.; Tanaka, I. *J. Phys. Chem.* **1975**, *79*, 2731–2734.
 (14) Shizuka, H.; Matsui, K.; Hirata, Y.; Tanaka, I. *J. Phys. Chem.* **1976**, *80*, 2070–2072.
 (15) Shizuka, H.; Matsui, K.; Hirata, Y.; Tanaka, I. *J. Phys. Chem.* **1977**, *81*, 2243–2246.
 (16) Shizuka, H.; Tsutsumi, K.; Jingui, M.; Tanaka, I. *Kokagaku Toronkai Koen Yoshishu* **1979**, 44–45; *chem. Abstr.* **1980**, *93*, 70604 u.
 (17) Nakagaki, R.; Kobayashi, T.; Nakamura, J.; Nagakura, S. *Bull. Chem. Soc. Jpn.* **1977**, *50*, 1909–1912.
 (18) Nakagaki, R.; Kobayashi, T.; Nagakura, S. *Bull. Chem. Soc. Jpn.* **1978**, *51*, 1671–1675.
 (19) Smith, K. K.; Kaufmann, K. J. *J. Phys. Chem.* **1978**, *82*, 2286–2291.
 (20) Betin, O. I.; Nurmukhametov, R. N.; Shigorin, D. N.; Loseva, M. V.; Chernova, N. I. *Bull. Acad. Sci. USSR, Phys. Ser. Engl. Transl.* **1978**, *42*, 73–76; *Izv. Akad. Nauk SSSR, Ser. Fiz.* **1978**, *42*, 533–538 and papers cited therein.
 (21) Barbara, P. F.; Rentzepis, P. M.; Brus, L. E. *J. Am. Chem. Soc.* **1980**, *102*, 2786–2791.
 (22) Barbara, P. F.; Brus, L. E.; Rentzepis, P. M. *J. Am. Chem. Soc.* **1980**, *102*, 5631–5635.
 (23) Ding, K.; Courtney, S. J.; Strandjord, A. J.; Flom, S.; Friedrich, D.; Barbara, P. F. *J. Phys. Chem.* **1983**, *87*, 1184–1188.
 (24) Mordziński, A.; Grabowska, A. *Chem. Phys. Lett.* **1982**, *90*, 122–127.
 (25) Rossetti, R.; Haddon, R. C.; Brus, L. E. *J. Am. Chem. Soc.* **1980**, *102*, 6913–6916.
 (26) Woolfe, G. J.; Thistlethwaite, P. J. *J. Am. Chem. Soc.* **1981**, *103*, 3849–3854.
 (27) Okada, T.; Karaki, I.; Mataga, N. *J. Am. Chem. Soc.* **1982**, *104*, 7191–7195.
 (28) Merritt, C.; Scott, G. W.; Gupta, A.; Yavrouian, A. *Chem. Phys. Lett.* **1980**, *69*, 169–173.
 (29) Huston, A. L.; Scott, G. W.; Gupta, A. *J. Chem. Phys.* **1982**, *76*, 4978–4985.
 (30) Flom, S. R.; Barbara, P. F. *Chem. Phys. Lett.* **1983**, *94*, 488–493.
 (31) Werner, T.; Kramer, H. E. A.; Kuester, B.; Herlinger, H. *Angew. Makromol. Chem.* **1976**, *54*, 15–29.
 (32) Werner, T.; Kramer, H. E. A. *Eur. Polym. J.* **1977**, *13*, 501–503.

(33) Kortuem, G.; Braun, W.; Herzog, G. *Angew. Chem.* **1963**, *75*, 653–661.

(34) Kroening, P.; Glandien, M. *Z. Phys. Chem. (Wiesbaden)* **1970**, *72*, 76–81.

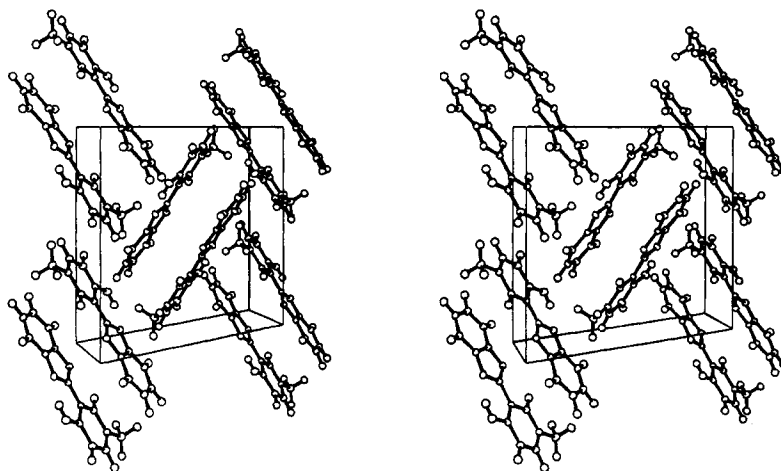


Figure 1. A stereoscopic projection⁴⁴ of the crystal packing of TIN.

The emission was observed perpendicularly to the excitation. The maximum absorbance of the solution did not exceed 0.15 in order to avoid innerfilter effects of the solute. For emission polarization measurements, the apparatus was set up in an "in line" arrangement³⁵ and equipped with a Glan-Thomson polarizer and a sheet polarizer (analyzer).³²

The fluorescence decay times were measured with the phase fluorimeter developed by Hauser et al.,³⁶⁻⁴⁰ the modulation frequencies being 100, 200, and 400 MHz. The degree of modulation of the emission signal was $\geq 10\%$.

Crystal Structure Determination of TIN. A $0.5 \times 0.5 \times 0.5$ mm³ crystal sealed in a thin-walled glass capillary and maintained at ca. 120 K was used for all X-ray diffraction measurements. The space-group is $P2_1/c$ with lattice parameters $a = 5.8082$ (8), $b = 12.683$ (1), $c = 16.502$ (2) Å, and $\beta = 120.523$ (8)° (lattice parameters resulted from refinement with 43 automatically centered 2θ values in the range from 31.29 to 42.41°, monochromatized Mo K α radiation); the chemical formula per asymmetric unit is C₁₃H₁₁N₃O.

Intensities were measured with a Syntex P1 autodiffractometer equipped with a low-temperature device (Syntex LT-1). Data were measured with an ω -scan technique for which the scan rate ranged from 2.0 to 24.0° min⁻¹ (depending on maximum reflection intensity) and the scan range was 0.75°; background radiation was measured on each side of the reflection ($\Delta\omega = 1.0^\circ$) for one-half the scan time. Reflections were measured to a resolution of $(\sin \theta/\lambda)_{\max} = 0.76$ Å⁻¹. The intensities were corrected for a systematic decrease in the intensity of three reference reflections (maximum 27%) and for Lorentz and polarization effects but not for absorption. Of the 3728 unique reflections measured, 2877 were classified as observed under the criterion $I \geq 3.0\sigma(I)$.

The initial crystal structure model was determined⁴¹ by direct methods and developed⁴² by difference Fourier and least-squares refinement techniques. Fractional atomic coordinates for all atoms, anisotropic temperature factors for all C, N, and O atoms, isotropic temperature factors for H atoms, and a single scale factor were refined. The following weighting scheme was used:

$$w = \{0.25 + \sigma^2(F) + 0.0125F_0 + 0.0001F_0^2 + 0.000001F_0^4\}^{-1}$$

(35) Parker, C. A. "Photoluminescence of Solutions"; Elsevier: Amsterdam, 1968; p 229.

(36) Woessner, G. Thesis, University of Stuttgart, 1983.

(37) Haar, H.-P.; Klein, U. K. A.; Hafner, F. W.; Hauser, M. *Chem. Phys. Lett.* **1977**, *49*, 563-567.

(38) Haar, H.-P.; Hauser, M. *Rev. Sci. Instrum.* **1978**, *49*, 632-633.

(39) Klein, U. K. A.; Haar, H.-P. *Chem. Phys. Lett.* **1979**, *63*, 40-42.

(40) Klein, U. K. A. Habilitationsschrift, University of Stuttgart, 1982.

(41) Main, P.; Lessinger, L.; Woolfson, M. M.; Germain, G.; Declercq, J.-P. "MULTAN 80, A System of Computer Programs for the Automatic Solution of Crystal Structures from X-ray Diffraction Data"; University of York: England, 1980.

(42) Stewart, J. M.; Machin, P. A.; Dickinson, C.; Ammon, H. L.; Heck, H. S.; Flack, H. "X RAY System—Version of 1976"; Technical Report TR-446, Computer Science Center, University of Maryland, College Park, MD, 1976.

TABLE I: Fractional Atomic Coordinates with Estimated Standard Deviations for TIN

atom	x	y	z
C(1)	0.5128 (3)	0.2767 (1)	0.4666 (1)
C(2)	0.6851 (3)	0.2270 (1)	0.4422 (1)
O(1)	0.7379 (3)	0.2629 (1)	0.37570 (9)
H(01)	0.648 (6)	0.319 (2)	0.353 (2)
C(3)	0.8105 (3)	0.1337 (1)	0.4891 (1)
H(3)	0.934 (5)	0.095 (2)	0.470 (2)
C(4)	0.7661 (3)	0.0920 (1)	0.5575 (1)
H(4)	0.850 (5)	0.019 (2)	0.587 (2)
C(5)	0.5935 (3)	0.1412 (1)	0.5819 (1)
C(M)	0.5536 (4)	0.0968 (1)	0.6585 (1)
H(1M)	0.386 (7)	0.132 (3)	0.653 (2)
H(2M)	0.686 (7)	0.142 (3)	0.719 (2)
H(3M)	0.558 (7)	0.010 (3)	0.662 (3)
C(6)	0.4669 (3)	0.2336 (1)	0.5350 (1)
H(6)	0.347 (5)	0.271 (2)	0.551 (2)
N(1)	0.3816 (3)	0.3727 (1)	0.42218 (9)
N(2)	0.2195 (3)	0.4220 (1)	0.44467 (9)
N(3)	0.4127 (3)	0.4171 (1)	0.35439 (9)
C(7)	0.2549 (3)	0.5041 (1)	0.3300 (1)
C(8)	0.2023 (3)	0.5827 (1)	0.2621 (1)
H(8)	0.293 (4)	0.580 (2)	0.226 (2)
C(9)	0.0227 (3)	0.6596 (1)	0.2520 (1)
H(9)	-0.014 (6)	0.725 (2)	0.207 (2)
C(10)	-0.1039 (3)	0.6608 (1)	0.3069 (1)
H(10)	-0.224 (5)	0.727 (2)	0.298 (2)
C(11)	-0.0505 (3)	0.5863 (1)	0.3745 (1)
H(11)	-0.141 (4)	0.584 (2)	0.412 (2)
C(12)	0.1334 (3)	0.5065 (1)	0.3858 (1)

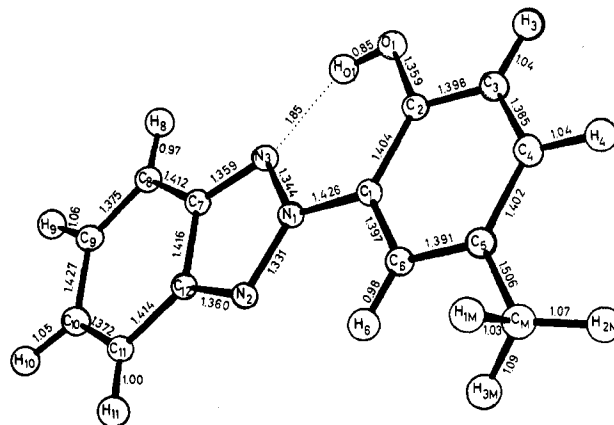


Figure 2. Bond distances for TIN at ca. 120 K. Estimated standard deviations are less than 0.0035 Å in bonds between nonhydrogen atoms and less than 0.055 Å in those involving H atoms.

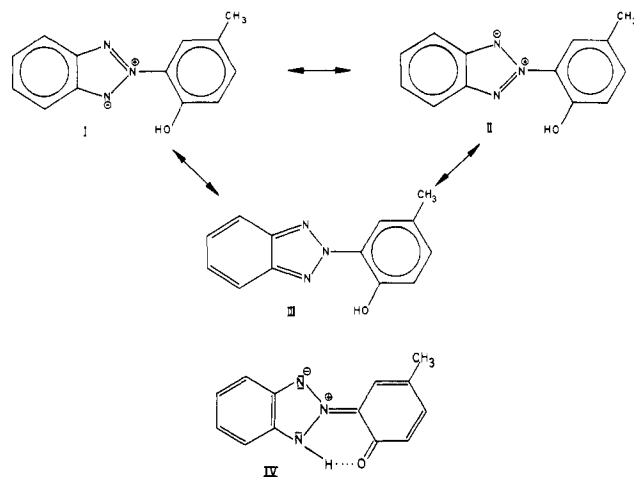
A total of 3398 reflections contributed to the refinement of 198 variables to give $R = 0.047$ and $R_w = 0.057$; the estimated standard deviation of an observation of unit weight is 1.16.

TABLE II: Least-Squares Mean Planes for TIN

plane 1:	N1, N2, N3, C7, C8, C9, C10, C11, C12 $\sigma = 0.015 \text{ \AA}$
plane 2:	C1, C2, O1, C3, C4, C5, CM, C6 $\sigma = 0.012 \text{ \AA}$
Equations in Orthogonal (\AA) Coordinates ^a	
plane 1:	$0.4739i + 0.5477j + 0.6895k = 6.1163$
plane 2:	$0.4805i + 0.5347j + 0.6952k = 6.0346$

^a The respective directions in the orthogonal coordinate system are related to those of the crystallographic system as follows: a , b^* , ($a \times b^*$). Interplanar angle 0.9° .

Scheme I



Results and Discussion

1. *Crystalline TIN as a Model for the Stabilizer Molecule with an Intramolecular Hydrogen Bond.* 1.1. *Crystal Structure Determination.* Fractional atomic coordinates are contained in Table I; temperature factors have been deposited as supplementary material (see paragraph at end of text regarding supplementary material). A stereoscopic packing diagram is presented in Figure 1; bond distances are in Figure 2. The molecule is almost perfectly planar (Table II). The angle of intersection between the normals of least-squares mean planes fit to the benzotriazole and the *p*-cresole moieties is 0.9° ; in MT⁴³ this value is approximately 57° . There is an intramolecular hydrogen bond in which the cresole hydroxyl group serves as the donor to atom N3 of the benzotriazole moiety (Figure 2). The bonding geometry (O—H = 0.85 (3), H...N = 1.85 (4), O—H...N = $149 (3)^\circ$) is typical for a N...H hydrogen bond.

The chemical structure of TIN has been described¹ as a resonance between three mesomeric forms (Scheme I). The observed bond distances demonstrate that form III predominates in the solid state. The influence of the intramolecular hydrogen bond results in preference of form I relative to II.

The conformation of TIN in the crystal is suitable for the formation of a tautomeric form, IV, which describes a partial charge transfer from the *p*-cresole to the benzotriazole moiety. As discussed earlier¹¹ this tautomer IV makes little or no significant contribution to the ground-state structure. However, its importance increases tremendously upon excitation (complete proton transfer in S_1' ,¹¹ calculated shift of charge densities in all excited states¹¹).

The crystal structure of 2-(2'-hydroxyphenyl)benzothiazole was reported by Stefson.⁴⁵

(43) Unpublished preliminary results for a crystal structure determination of MT for which there are two molecules per asymmetric unit.

(44) Johnson, C. K. Report ORNL-5138, Oak Ridge National Laboratory, Oak Ridge, TN, 1971.

(45) Stenson, P. *Acta Chem. Scand.* **1970**, *24*, 3729–3738.

(46) Engelman, R.; Jortner, J. *Mol. Phys.* **1980**, *18*, 145–164.

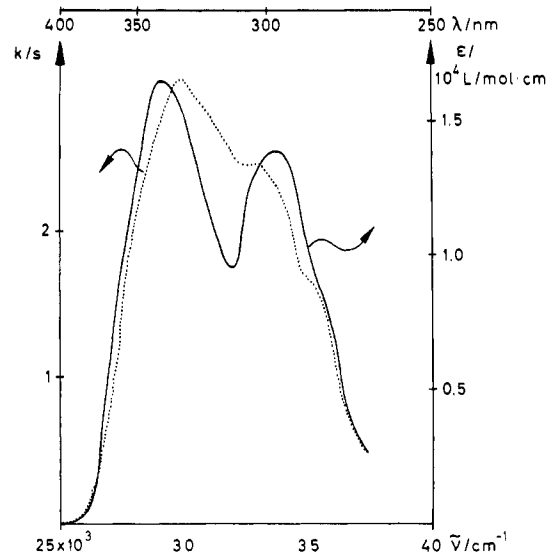


Figure 3. Absorption spectrum of TIN in *n*-heptane (—), $C_{\text{TIN}} = 1 \times 10^{-4} \text{ M}$, $T = 298 \text{ K}$; reflection spectrum of TIN (10^{-3} m on SiO_2) (...).

1.2. *Comparison of the Absorption Spectrum of TIN in Hydrocarbon Solutions with the Reflection Spectrum of TIN Adsorbed on Silica Gel.* The absorption spectrum of TIN in hydrocarbon solutions of different viscosities (ranging from isopentane with $\eta_{298\text{K}} = 0.223 \times 10^{-3}$ to liquid paraffin with $\eta_{298\text{K}} = 251 \times 10^{-3} \text{ kg m}^{-1} \text{ s}^{-1}$ (=Pa s)) are identical. Figure 3 shows the absorption spectrum of TIN in *n*-heptane and the reflection spectrum of TIN adsorbed on SiO_2 . Two bands appear whose positions differ only slightly.

The resolution of the reflection spectrum is lower than that of the absorption spectrum. The ratio of the intensity of both absorption bands is temperature independent and corresponds to the intensity ratio in the reflection spectrum. From this the conclusion can be drawn that the absorption transitions are the same for TIN in the crystalline state and in fluid hydrocarbon solution.

1.3. *Emission Spectra of TIN in the Crystalline State and in Solid Hydrocarbon Matrices.* The fluorescence of TIN (intra) in hydrocarbons ($\lambda_{\text{max}} = 638 \text{ nm}$,^{11,12} $S_1' \rightarrow S_0'$ in Figure 4) can only be observed below the glass temperature of the solvent. The quantum yield is 2×10^{-4} at 77 K.⁵ In carefully dried hydrocarbon solutions only the long wavelength fluorescence ($\lambda_{\text{max}} = 638 \text{ nm}$) exists. The fluorescence with a normal Stokes shift ($\lambda_{\text{max}} \approx 390 \text{ nm}$)^{11,12} and mirror imaged to the absorption spectrum is not obtained in these solvents in accordance with Flom and Barbara.³⁰ We confirm the observation of these authors that moisture in hydrocarbon solutions of TIN is responsible for the appearance of the short wavelength fluorescence. In polar solvent at least part of the TIN molecules change from being intramolecularly to intermolecularly hydrogen bonded to solvent molecules as revealed from the change in the absorption, emission, and emission excitation spectra.^{11,12} Thus, the short wavelength fluorescence ($\lambda = 390 \text{ nm}$ in EEP^{11,12}) and the phosphorescence originate from the intermolecularly hydrogen-bonded form while the fluorescence at $\lambda_{\text{max}} = 638 \text{ nm}$ is due to the intramolecularly hydrogen-bonded form.^{11,12}

The nonplanar MT molecule is considered to be a model for the intermolecularly hydrogen-bonded TIN molecule, since it shows the same shape of emissions (fluorescence and phosphorescence).^{11,12} This will be reported in a forthcoming paper.

The crystalline TIN also emits only in the long wavelength region, the position and the shape of the emission being identical with those in hydrocarbon solutions. However, the intensity of the emission of the crystalline TIN is sufficient to measure the relative quantum yields and the fluorescence decay times throughout the temperature range from 77 to 350 K.

(47) Woolfe, G. J.; Melzig, M.; Schneider, S.; Doerr, F. *Chem. Phys.* **1983**, *77*, 213–221.

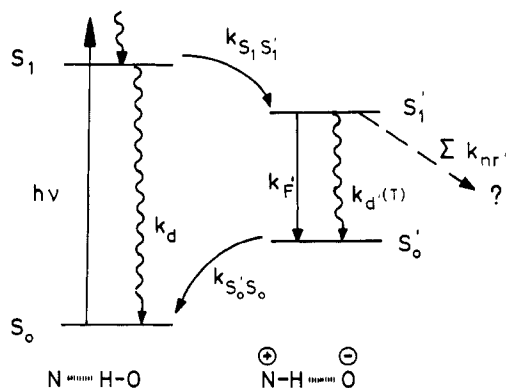


Figure 4. Scheme of energy dissipation of TIN(intra): $k_{S_0'S_0}$, $k_{S_1'S_1'}$, rate constants of intramolecular proton transfer processes in the ground and first excited singlet state; k_F' , rate constant of fluorescence emission from S_1' ; k_d , $k_d'(T)$, $\Sigma k_{nr}'$, rate constants of radiationless deactivation processes of S_1 , of S_1' , and reaction channels of S_1' (temperature independent).

Based on the results of the X-ray crystal structure determination and because the emission of TIN in hydrocarbon solution and in the crystalline state is identical, crystalline TIN can be considered as a model for the stabilizer molecule with an intramolecular hydrogen bond (TIN(intra)).

1.4. Energy Transfer in Crystalline TIN. The prerequisite for energy transfer (overlap of absorption and emission spectrum of acceptor and donor) is fulfilled only for the S_1 excited state of TIN(intra) (see Figure 4) but not for S_1' . The trivial case of emission and reabsorption can be excluded since no efficient emission process from the S_1 state exists due to its short lifetime ($\tau \leq 10$ ps); no S_1 emission was detected in crystalline TIN. However, radiationless energy transfer in crystalline TIN including the S_1 states seems to be feasible. In this case the lifetime of the excited molecule has to be replaced by the lifetime of the excitons. The deactivation processes of S_1 (e.g., k_d and $k_{S_1'S_1'}$, Figure 4) still exist and have to be attributed to the single molecule and not to the crystal.

The question concerning the existence of excitons will be addressed after the deactivation processes competing with the proton transfer have been discussed.

2. Influence of Temperature and Isotope Exchange on the Transfer of Proton/Deuteron in the S_1 State of TIN(intra). In principle, phase fluorimetry gives informations about population and depopulation of the emitting state (here $S_1' \rightarrow S_0'$, Figure 4). For crystalline TIN, however, only one time constant (decay of S_1' fluorescence) was found in the temperature range from 77 to 350 K which means that the population rate of the emitting state S_1' is higher than the time resolution of the phase fluorimeter.⁴⁸ Therefore, the proton/deuteron transfer should be faster $\geq 10^{11}$ s⁻¹. This is in agreement with the results of Flom and Barbara³⁰ who found the same limit for the transfer rate constant in fluid hydrocarbon solutions of TIN. Since the rate of population of S_1' is much higher than its decay rate, the lifetime of the S_1' state provides exact information about the S_1' decay kinetics without being disturbed by the S_1' formation kinetics. Therefore, the observed deuterium isotope effect and the temperature de-

(48) From the reaction scheme (Figure 4) the following expression for the phase angle of $S_1' \rightarrow S_0'$ fluorescence can be derived:

$$\omega \cot \chi = \frac{(k_F' + k_d' + \Sigma k_{nr}') (k_F' + k_d + k_{S_1'S_1'}) - \omega^2}{k_F' + k_d' + \Sigma k_{nr}' + k_F + k_d + k_{S_1'S_1'}}$$

In the reaction scheme, k_F was omitted since $k_F \ll k_d + k_{S_1'S_1'}$. Moreover, $k_F + k_d' + \Sigma k_{nr}' \ll k_d + k_{S_1'S_1'}$. Denoting $(k_F' + k_d' + \Sigma k_{nr}')^{-1} = \tau'$ we get

$$\omega \cot \chi \approx 1/\tau' - \frac{\omega^2}{k_d + k_{S_1'S_1'}}$$

Experimentally, $\omega \cot \chi$ was found to be constant at all frequencies 25 MHz $\leq \omega/2\pi \leq 400$ MHz within $\pm 2\%$. With this from $\tau' \approx 200$ ps (cf. Figure 5, room temperature) it may be concluded (e.g., with $\omega = 2\pi \times 400$ MHz) that $1/(k_d + k_{S_1'S_1'}) \leq 16$ ps, which means S_1' is formed from S_1 within that time.

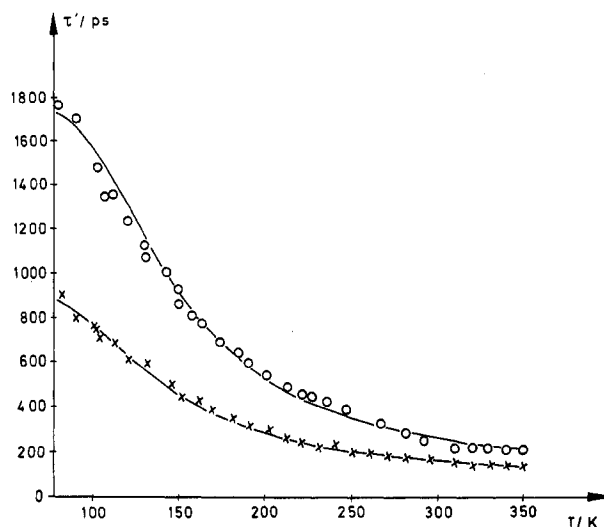


Figure 5. Lifetimes of τ' of the S_1' fluorescence of crystalline TIN(H) (x) and TIN(D) (o) vs. temperature: $\lambda_{exc} = 350 + 357$ (Kr laser), $\lambda_{obsd} = 638$ nm; the curves are calculated from the parameters given in Table III.

TABLE III: Parameters for the Calculated Curves $\tau'(T)$ (Eq 1 and 2) of Crystalline TIN(H) and TIN(D) (Figure 5)

	TIN(H)	TIN(D)
$k_0', 10^8 \text{ s}^{-1}$	11 ± 1	5.7 ± 0.5
$\tau_0' = 1/k_0', \text{ ps}$	900 ± 90	1760 ± 180
k_d'		
$A, 10^{10} \text{ s}^{-1}$	3.0 ± 0.3	2.3 ± 0.2
$E, \text{ kJ/mol}$	3.98 ± 0.20	4.61 ± 0.23

pendence of the lifetime τ' of S_1' are considered not to be influenced by eventual isotope or temperature effects on the lifetime of its precursor S_1 .

2.1. The S_1' Decay Kinetics. The temperature dependence of the fluorescence decay time τ' of S_1' can be described by eq 1

$$1/\tau' = k_0' + k_d'(T) \quad (1)$$

whereby k_0' represents the sum of the temperature-independent processes while $k_d'(T)$ is given to a first approximation by the Arrhenius expression eq 2 (see Figure 4). Figure 5 shows the

$$k_d'(T) = A \exp(-E/RT) \quad (2)$$

lifetimes τ' of crystalline protonated and deuterated TIN (TIN(H) and TIN(D)) in the temperature range from 77 to 350 K. The curves were obtained by adjusting the parameters given in Table III to the experimental results. As Figure 5 demonstrates the temperature dependence of τ' can be satisfactorily described by eq 1 and 2. (Note added in proof: Meanwhile we have measured the lifetimes τ' in the range from 77 to 10 K for crystalline TIN(H) and TIN(D). Both lifetimes τ' increase continuously in this temperature range.)

2.2. Discussion of the Parameters; Deuterium Effect on the S_1' Decay Kinetics. The error in k_0' and A (Table III) obtained by the above-mentioned fitting procedure to the experimental points (Figure 5) is $< \pm 10\%$ while the error in the activation energy is $< \pm 5\%$.

The isotope effect on the temperature-dependent rate constant $k_d'(T)$ is relatively small: the preexponential factor A decreases slightly whereas the activation energy E increases upon deuteration (Table III). On the whole the temperature-dependent deactivation process $k_d'(T)$ is slower in TIN(D) than in TIN(H). Yet a marked isotope effect on the temperature-independent rate constant k_0' is observed (Table III). k_0' (H) is higher than k_0' (D) by a factor of 2. The lifetimes expected from these constants for very low temperature are 900 ps for TIN(H) and 1760 ps for TIN(D). The temperature-independent constant k_0' includes at least the emission rate constant k_F' , eq 3. An isotope effect on

$$k_0' = k_F' + \Sigma k_{nr}' \quad (3)$$

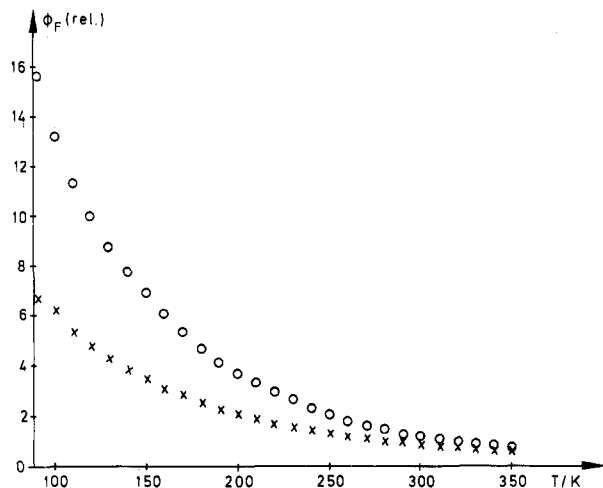


Figure 6. Relative overall quantum yield $\Phi_F(\text{rel.})$ of the S_1' fluorescence of crystalline TIN(H) (X) and TIN(D) (O) vs. temperature; $\lambda_{\text{exc}} = 366$ nm, $\lambda_{\text{obsd}} = 638$ nm.

k_F' is improbable since the corresponding emission spectra of TIN(H) and TIN(D) are identical. Therefore, the isotope effect has to be related to radiationless and temperature-independent deactivation channels ($\Sigma k_{nr}'$). A lower limit of the quantum yield of $\Sigma k_{nr}'$ can be evaluated from the difference of the k_0' values of TIN(H) and TIN(D) and the lifetime τ' of TIN(H):

$$\Sigma \Phi_{nr}'^H \geq (k_0'^H - k_0'^D) \tau_{H'}' \quad (4)$$

$$T = 77 \text{ K: } \Sigma \Phi_{nr}'^H \geq 0.48 \quad (5)$$

$$T = 296 \text{ K: } \Sigma \Phi_{nr}'^H \geq 0.07 \quad (6)$$

2.3. Kinetics of the Proton/Deuteron Transfer. The processes responsible for the depopulation of S_1 are faster by about two orders of magnitude ($\tau \geq 10$ ps even at 77 K) than those of S_1' described in section 2.2. If we take into account the known deactivation rates of the S_1' state the measured overall quantum yield Φ_F of the S_1' fluorescence as a function of temperature (Figure 6) gives information about the decay kinetics of the S_1 state. For Φ_F the following equation holds

$$\Phi_F = \Phi_{Tr} \Phi_{F'} = \Phi_{Tr} k_{F'}' \tau' \quad (7)$$

whereby Φ_{Tr} is the proton transfer yield from S_1 to S_1' and $\Phi_{F'}$ the intrinsic fluorescence quantum yield of S_1' . Since only relative values are available for Φ_F , eq 7 is modified to

$$\frac{\Phi_F^X}{\Phi_F^Y} = \frac{\Phi_{Tr}^X \tau_X'}{\Phi_{Tr}^Y \tau_Y'} \quad (8)$$

whereby the unknown $k_{F'}'$ is eliminated. The indices X and Y mean H and D when the isotope effect and T_1 and T_2 when the temperature effect is considered. The above-described elimination of $k_{F'}'$ seems to be justified since it remains constant (assuming neither isotope nor temperature effect on $k_{F'}'$).

Rearranging of eq 8 gives

$$\frac{\Phi_{Tr}^X}{\Phi_{Tr}^Y} = \frac{\Phi_F^X \tau_Y'}{\Phi_F^Y \tau_X'} \quad (9)$$

to describe the influence of temperature and isotope exchange on the transfer yield Φ_{Tr} . From Table IV the following value is found for the isotope effect on Φ_{Tr} at 296 K:

$$\Phi_{Tr}^H / \Phi_{Tr}^D = 1.03 \pm 0.14 \quad (10)$$

i.e., there is *no isotope effect* on the transfer yield within experimental error, or

$$\Phi_{Tr}^H = \Phi_{Tr}^D \quad (11)$$

TABLE IV: Isotope Effect on the Lifetime τ' and the Overall Quantum Yield Φ_F of the S_1' State of Crystalline TIN(intra) at 296 K

	τ' , ^a ps	τ_D' / τ_H'	Φ_F^H / Φ_F^D	$\Phi_{Tr}^H / \Phi_{Tr}^D$
TIN(H)	141 ± 8			
TIN(D)	243 ± 22	1.72 ± 0.18	0.60 ± 0.05	1.03 ± 0.14

^a The lifetimes are calculated from the parameters of Table III.

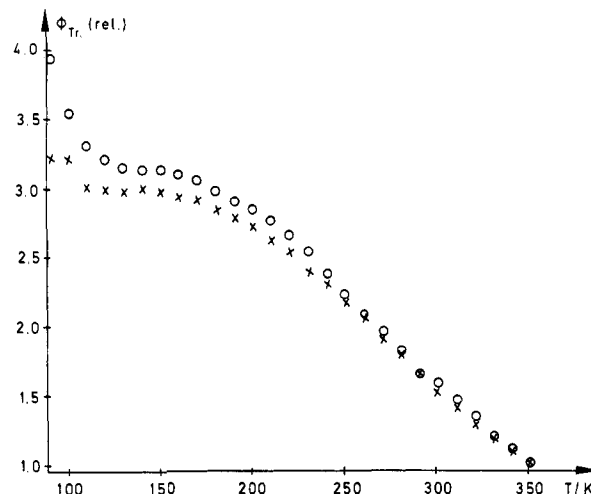


Figure 7. Relative proton/deuteron transfer yield $\Phi_{Tr}(\text{rel.})$ of crystalline TIN(H) (X) and TIN(D) (O) as a function of temperature, $\Phi_{Tr}(\text{rel.}) = 1$ at 350 K.

With eq 11 and the definition of the transfer yield one finds (for notations see Figure 4)

$$\frac{k_{S_1, S_1'}^H}{k_d^H + k_{S_1, S_1'}^H} = \frac{k_{S_1, S_1'}^D}{k_d^D + k_{S_1, S_1'}^D} \quad (12)$$

or

$$\frac{k_{S_1, S_1'}^H}{k_{S_1, S_1'}^D} = \frac{k_d^H + k_{S_1, S_1'}^H}{k_d^D + k_{S_1, S_1'}^D} \quad (13)$$

$k_{S_1, S_1'}$, k_d being the rate constants of proton transfer ($S_1 \rightarrow S_1'$) and of the radiationless deactivation of S_1 for TIN(intra). Equation 13 allows two interpretations: (i) $k_d^H, k_d^D \ll k_{S_1, S_1'}^H, k_{S_1, S_1'}^D$, i.e., the proton/deuteron transfer is the only deactivation channel of S_1 , or in other words, the transfer yield $\Phi_{Tr} = 1$ (see section 2.4); (ii) the radiationless deactivation (k_d) and the transfer process ($k_{S_1, S_1'}$) are either *uninfluenced* or are influenced in the same manner by the isotope exchange. The temperature dependence of Φ_{Tr} provides a basis upon which to decide between i and ii.

2.4. Influence of Temperature on the Transfer Yield for TIN(H) and TIN(D). Figure 7 presents the variation of the relative transfer yield ($\Phi_{Tr}(\text{rel.}) = 1$ at 350 K) of crystalline TIN(H) and TIN(D) with temperature. The transfer yields of both substances behave similarly. With decreasing temperature a steep rise of the transfer yield is observed followed by a flattening below 160 K. The transfer yields at low temperature are higher by a factor of about 3 compared to those for 350 K. This means that the *transfer yields at room temperature and above are considerably smaller than 1*. With this taken into account suggestion i in section 2.3 has to be discarded and only suggestion ii is consistent with a transfer yield < 1 . In summation, *no isotope effect on the transfer yield* was found. If an isotope effect exists at all both the proton transfer $k_{S_1, S_1'}$ and the competing process (k_d) are influenced in the same manner. It follows that the process k_d competing with the proton transfer is temperature dependent and its quantum yield amounts at least to 0.5 at room temperature. A temperature dependence of the proton transfer rate constant $k_{S_1, S_1'}$ cannot be excluded; however, if there is an activation energy at all it must be significantly smaller than that of the competing process k_d .

3. *The S₁ State.* The question of whether or not the competing process k_d is related to exciton states cannot yet be answered. Shizuka et al.¹⁵ report on radiationless processes competing with proton transfer even in *fluid* solution.

Fluorescence from the S₁ state is not observed for TIN(*intra*) which means that k_F is not an effective deactivation process. In polar solvents, however, TIN(*inter*) molecules with an intermolecular hydrogen bond to the solvent show S₁ fluorescence,^{11,12} a forthcoming paper will report on the decay of S₁ of TIN(*inter*).

The results of TIN(*intra*) correspond very well to the investigations of Shizuka et al.¹³⁻¹⁶ concerning substituted 6-(2-hydroxy-5-methylphenyl)-*s*-triazine: (i) there is no isotope effect on proton transfer yield; (ii) there is no potential barrier for proton transfer; and (iii) the radiationless decay k_d has an activation energy of 2-3 kcal/mol.¹⁵

On the other hand, according to Mordziński and Grabowska²⁴ 2-(2-hydroxyphenyl)benzoxazole shows interesting differences in comparison with TIN(*intra*): (i) the isotope effect on Φ_T , amounts to 1.45 below 163 K; (ii) there is no temperature dependence of Φ_T , in the range from 263 to 163 K; and (iii) there is no isotope effect on the fluorescence decay time τ' on S₁'. Neither Huston et al.²⁹ nor Flom and Barbara³⁰ detected a long-lived intermediate using transient absorption spectrometry. Hence, an effective population of the triplet of TIN(*intra*) from the S₁ state can be excluded.

4. *The S₁' State.* The lifetime τ' of S₁' of TIN(*intra*) is considerably longer than of its precursor S₁. S₁' emits, though with low quantum yield, whereas no emission from S₁ of TIN(*intra*) is observed. Since the energy gap between the excited state and the ground state decreases upon proton transfer by about 10000 cm⁻¹ (Figure 4) one expects $\tau > \tau'$ according to the energy-gap law.⁴⁶ However, the opposite holds. Hence, the processes k_d and k_d' are thought to have different character.

The radiationless process k_d' depends on temperature and provides a small isotope effect. Fluorescence quenching of S₁' by rotation of the cresole group should not be effective in TIN(*intra*)¹² due to its short lifetime (≈ 140 ps at 296 K). Besides that the intramolecular hydrogen bond and the double bond character of the C-N bond between the cresole and the benzotriazole moieties (which increases upon excitation; see ref 47 for the corresponding benzoxazole) might hinder a torsional motion drastically. In this context it should be mentioned that the absorption spectra of TIN(*intra*) in hydrocarbons are independent

of viscosity and correspond to the reflection spectrum (section 1.2).

Due to the lack of the intramolecular hydrogen bond the MT molecule is not planar, see section 1.1.

In addition to the emission process k_F' at least one temperature-independent channel k_{nr}' (Figure 4) exists which is responsible for the isotope effect found for the lifetime S₁' (for the estimation of its quantum yield see eq 4-6).

Conclusions

The intramolecular hydrogen bond of TIN is a prerequisite for the rapid radiationless deactivation of the excited state and hence for its applicability as UV stabilizer. The crystal structure determination revealed a relatively strong intramolecular hydrogen bond and indicated the importance of structure III, Scheme I. Crystalline TIN shows only the fluorescence of the proton transferred species S₁' with a large Stokes shift (Figure 4). The overall quantum yield of this emission exhibits an increase upon deuteration. This deuteration effect, however, stems exclusively from the fluorescence decay time τ' while the yield of proton transfer shows no isotope effect (90-350 K). The proton transfer yield is considerably lower than 1 at room temperature which means that a very effective quenching process of the precursor S₁ exists, in agreement with the fact that no fluorescence from the S₁ state of TIN(*intra*) is observed. The S₁ fluorescence arises, however, in polar solvents from those molecules where the *intra*molecular hydrogen bond is changed to an *inter*molecular hydrogen bond to the solvent.

Acknowledgment. We express our sincere thanks to Prof. Dr. A. Grabowska and Prof. Dr. Z. R. Grabowski, Warsaw, for an interesting discussion. Further thanks are due to Dr. T. Werner, Bayer AG., Leverkusen, for helpful suggestions, and to Dr. Helmut Mueller, CIBA-GEIGY, Basel, for providing us samples, and to Prof. Dr. H. Herlinger and Dr. D. Fiebig, Stuttgart, for the use of their reflection spectrometer. The financial support of the Deutsche Forschungsgemeinschaft and of the Fonds der Chemischen Industrie is gratefully acknowledged.

Registry No. TIN (H), 2440-22-4; TIN (D), 85775-60-6; MT, 58380-86-2; deuterium, 7782-39-0.

Supplementary Material Available: Refined temperature factors and calculated and observed structure factors are available (25 pages). Ordering information is given on any current masthead page.